Pygmy resonances and neutron skins

J. Piekarewicz

Phys. Rev. C **83**, 034319 — Published 24 March 2011

DOI: 10.1103/PhysRevC.83.034319

Pygmy Resonances and Neutron Skins

J. Piekarewicz[1]

[1]*Department of Physics, Florida State University, Tallahassee, FL 32306*

Motivated by a recent experiment, the distribution of electric dipole strength in the neutron-rich ^{68}Ni isotope was computed using a relativistic random phase approximation with a set of effective interactions that—although well calibrated—predict significantly different values for the neutron-skin thickness in ^{208}Pb. The emergence of low-energy "Pygmy" strength that exhausts about 5-8% of the energy weighted sum rule (EWSR) is clearly identified. In addition to the EWSR, special emphasis is placed on the dipole polarizability. In particular, our results suggest a strong correlation between the dipole polarizability of ^{68}Ni and the neutron-skin thickness of ^{208}Pb. Yet we find a correlation just as strong and an even larger sensitivity between the neutron-skin thickness of ^{208}Pb and the *fraction* of the dipole polarizability exhausted by the Pygmy resonance. These findings suggest that the dipole polarizability may be used as a proxy for the neutron skin.

PACS numbers: 21.10.-k,21.10.Re,21.60.Jz

I. INTRODUCTION

The determination of the neutron radius of a heavy nucleus is a problem of fundamental importance that has been raised to a place of prominence due to its far reaching implication in areas as diverse as atomic parity violation [1, 2], nuclear structure [3–7], heavy-ion collisions [8–12], and neutron-star structure [13–18]. Earlier attempts at mapping the neutron distribution of heavy nuclei were met with skepticism as they relied on strongly-interacting processes that are handicapped by large and controversial uncertainties in the reaction mechanism [19, 20]. Instead, the enormously successful parity-violating program at the Jefferson Laboratory provides an attractive electroweak alternative. The Lead Radius experiment (PREx) aims to determine the neutron radius of ^{208}Pb accurately and model independently using parity-violating electron scattering [21, 22]. Parity violation at low momentum transfers is particularly sensitive to the neutron distribution because the neutral weak-vector boson Z^0 couples preferentially to the neutrons. Moreover, the parity-violating asymmetry, although very small, may be interpreted with as much confidence as conventional electromagnetic scattering experiments that have been used for decades to map the proton distribution with exquisite accuracy. The Lead Radius experiment was successfully commissioned in March of 2010. High quality data were collected at the designed luminosity and with sufficient statistics to provide (likely by the Spring of 2011) a significant first experimental constraint on the neutron radius of ^{208}Pb [22].

A promising complementary approach to the parity-violating program relies on the electromagnetic excitation of the electric dipole mode [23]. For stable (medium to heavy) nuclei with a moderate neutron excess the dipole response is concentrated on a single fragment—*the giant dipole resonance (GDR)*—that exhausts almost 100% of the classical Thomas-Reiche-Kunz (TRK) sum rule. For this mode of excitation—perceived as an oscillation of neutrons against protons—the symmetry energy acts as its restoring force. Models with a soft symmetry energy, namely, ones that change slowly with density, predict large values for the symmetry energy at the densities of relevance to the excitation of this mode. As a consequence, the stronger restoring force of the softer models generates a dipole response that is both hardened (*i.e.,* pushed to higher excitation energies) and quenched relative to its stiffer counterparts. Given that the neutron radius of a heavy nucleus is also sensitive to the density dependence of the symmetry energy, the peak position of the GDR may be used as a (mild) constrain on the neutron radius.

A more stringent constrain on the neutron radius is expected to emerge as the nucleus develops a neutron-rich skin. Concomitant with the development of a neutron skin is the appearance of low energy dipole strength—the so-called *pygmy dipole resonance (PDR)* [24–30]. Thus, it has been suggested that the PDR—perceived as an excitation of the neutron-rich skin against the symmetric core—may be used as a constraint on the neutron skin of heavy nuclei [31]. In particular, the *fraction* of the energy weighted sum rule (EWSR) exhausted by the pygmy resonance has been shown to be sensitive to the neutron-skin thickness of heavy nuclei [31–35]. Recent pioneering experiments on unstable neutron-rich isotopes in Sn, Sb, and Ni seem to support this assertion [34, 36, 37].

The main goals of this manuscript are twofold. First, to use the recently measured distribution of Pygmy dipole strength in ^{68}Ni [37] to confirm our earlier assertion that models with overly large neutron skins—and thus stiff symmetry energies—are in conflict with experiment [31]. Second, to explore possible correlations between the neutron-skin thickness in ^{208}Pb and the *dipole polarizability*. This is motivated by a recent work by Reinhard and Nazarewicz that suggests that *the neutron skin is strongly correlated with the dipole polarizability but very weakly correlated with the low-energy electric dipole strength* [38].

Regarding the first goal, a significant first step was recently taken by Carbone and collaborators [35]. Using the

fraction of the EWSR exhausted by the Pygmy resonance in both ^{68}Ni [37] and ^{132}Sn [36], the slope of the symmetry energy was constrained to the range $L=64.8\pm15.7$ MeV. This constrain appears to rule out about half of the 26 effective interactions—including all relativistic ones—considered in their work. Viewed in this context, our contribution is a modest one, as we will limit ourselves to a smaller set of exclusively relativistic mean-field interactions. However, we will show that some modern relativistic effective interactions are soft enough to fall comfortably within the proposed range of L. Concerning the second goal, the claim by Reinhard and Nazarewicz [38] is particularly intriguing given that the dipole polarizability is proportional to the *inverse energy weighted sum* of the dipole response. As such, the dipole polarizability weighs more heavily the low-energy (Pygmy) than the high-energy (Giant) part of the response. So whereas the percentage of the EWSR exhausted by the Pygmy amounts to a meager 5-8%, its contribution to the dipole polarizability can reach values as high as 20-25%. So how can the neutron-skin thickness of ^{208}Pb be strongly correlated to the dipole polarizability but weakly correlated to the low-energy dipole strength? This is a question well worth exploring. Note that in this work we will not address whether the PDR is collective or not (for some recent reviews see Refs. [39, 40]). We believe that independent of the nature of the mode, the emergence of low-energy dipole strength as nuclei develop a neutron-rich skin is an incontrovertible fact.

The manuscript has been organized as follows. In Sec. II we introduce the formalism used in this work paying special attention to the various moments of the dipole response. In Sec. III results are presented for the distribution of dipole strength using relativistic effective interactions that span a wide range of values for the neutron-skin thickness of ^{208}Pb. We end by summarizing our results in Sec. IV.

II. FORMALISM

The starting point for the calculation of the nuclear response is the interacting Lagrangian density of Ref. [41] supplemented by an isoscalar-isovector term originally introduced in Ref. [13]. That is,

$$\begin{aligned}\mathscr{L}_{\rm int} &= \bar{\psi}\left[g_{\rm s}\phi-\left(g_{\rm v}V_\mu+\frac{g_\rho}{2}\boldsymbol{\tau}\cdot\mathbf{b}_\mu+\frac{e}{2}(1+\tau_3)A_\mu\right)\gamma^\mu\right]\psi \\ &- \frac{\kappa}{3!}(g_{\rm s}\phi)^3-\frac{\lambda}{4!}(g_{\rm s}\phi)^4+\frac{\zeta}{4!}g_{\rm v}^4(V_\mu V^\mu)^2+\Lambda_{\rm v}\left(g_\rho^2\,\mathbf{b}_\mu\cdot\mathbf{b}^\mu\right)\left(g_{\rm v}^2V_\nu V^\nu\right)\,. \end{aligned} \tag{1}$$

The Lagrangian density includes an isodoublet nucleon field (ψ) interacting via the exchange of two isoscalar mesons, a scalar (ϕ) and a vector (V^μ), one isovector meson (b^μ), and the photon (A^μ) [42, 43]. In addition to meson-nucleon interactions the Lagrangian density is supplemented by four nonlinear meson interactions with coupling constants denoted by κ, λ, ζ, and $\Lambda_{\rm v}$. The first two terms (κ and λ) are responsible for a softening of the equation of state of symmetric nuclear matter at normal density [44]. This softening results in a significant reduction of the compression modulus of nuclear matter relative to the original Walecka model [42, 44, 45] that is demanded by the measured distribution of isoscalar monopole strength in medium to heavy nuclei [46–49]. Further, omega-meson self-interactions, as described by the parameter ζ, also serve to soften the equation of state of symmetric nuclear matter but at much higher densities. Finally, $\Lambda_{\rm v}$ induces isoscalar-isovector mixing and is responsible for modifying the poorly-constrained density dependence of the symmetry energy [13, 14]. Tuning this parameter has served to uncover correlations between the neutron radius of a heavy nucleus (such as ^{208}Pb) and a host of both laboratory and astrophysical observables.

The first step in a consistent mean-field plus RPA (MF+RPA) approach to the nuclear response is the calculation of various ground-state properties. This procedure is implemented by solving the equations of motion associated with the above Lagrangian density in a self-consistent, mean-field approximation [42]. For the various meson fields one must solve Klein-Gordon equations with the appropriate baryon densities appearing as their source terms. These baryon densities are computed from the nucleon orbitals that are, in turn, obtained from solving the one-body Dirac equation in the presence of scalar and time-like vector potentials. This procedure must then be repeated until self-consistency is achieved. What emerges from such a calculation is a set of single-particle energies, a corresponding set of Dirac orbitals, and scalar and time-like vector mean-field potentials. A detailed implementation of this procedure may be found in Ref. [50].

Having computed various ground-state properties one is now in a position to compute the linear response of the mean-field ground state to a variety of probes. In the present case we are interested in computing the electric dipole ($E1$) response as probed, for example, in photoabsorption experiments. Although the MF+RPA calculations presented here follow closely the formalism developed in much greater detail in Ref. [47], some essential details are repeated here for completeness.

The isovector dipole response of interest may be extracted from the imaginary part of a suitable polarization tensor.

That is,

$$S_L(q,\omega) = \sum_n \Big|\langle\Psi_n|\hat{\rho}(\mathbf{q})|\Psi_0\rangle\Big|^2 \delta(\omega-\omega_n) = -\frac{1}{\pi}\Im\,\Pi^{00}_{33}(\mathbf{q},\mathbf{q};\omega)\ , \tag{2}$$

where Ψ_0 is the exact nuclear ground state and Ψ_n is an excited state with excitation energy $\omega_n = E_n - E_0$. To excite electric-dipole modes a transition operator of the following form is used:

$$\hat{\rho}(\mathbf{q}) = \int d^3r\,\bar{\psi}(\mathbf{r}) e^{-i\mathbf{q}\cdot\mathbf{r}}\gamma^0\tau_3\psi(\mathbf{r})\ . \tag{3}$$

Here $\hat{\rho}(\mathbf{q})$ is the Fourier transform of the timelike-isovector density, $\tau_3 = \mathrm{diag}(1,-1)$ is the third isospin matrix, and $\gamma^0 = \mathrm{diag}(1,1,-1,-1)$ is the zeroth (or timelike) component of the Dirac matrices. Such a transition operator is capable of exciting all natural-parity states. In the present work we are interested in the study of electric dipole modes so one must project out the $J^\pi = 1^-$ component of the transition operator. That is,

$$\hat{\rho}_\mu(\mathbf{q}) = -4\pi i Y^*_{1\mu}(\hat{\mathbf{q}}) \int d^3r\,\bar{\psi}(\mathbf{r}) j_1(qr) Y_{1\mu}(\hat{\mathbf{r}})\gamma^0\tau_3\psi(\mathbf{r})\ , \tag{4}$$

where j_1 is a spherical Bessel function and $Y_{1\mu}$ are spherical harmonics. To compare against experiment and to make contact with the classical TRK sum rule we compute the response in the long-wavelength approximation. Namely, we assume $j_1(qr) \approx qr/3$ so that the transition density reduces to

$$\hat{\rho}_\mu(\mathbf{q}) \underset{qr\ll 1}{=} -\frac{4\pi}{3} i q Y^*_{1\mu}(\hat{\mathbf{q}}) \int d^3r\,\bar{\psi}(\mathbf{r}) r Y_{1\mu}(\hat{\mathbf{r}})\gamma^0\tau_3\psi(\mathbf{r}) \equiv -\frac{4\pi}{3} \imath q Y^*_{1\mu}(\hat{\mathbf{q}}) \mathscr{M}(E1,\mu)\ , \tag{5}$$

where $\mathscr{M}(E1,\mu)$ is the isovector-dipole moment [23]. In the long-wavelength limit, the distribution of isovector dipole strength $R(\omega;E1)$ may be directly extracted from the longitudinal response. That is,

$$\lim_{q\to 0} S_L(q,\omega;E1) = \frac{4\pi}{9} q^2 R(\omega;E1)\ . \tag{6}$$

where

$$R(\omega;E1) = 3\sum_n \langle 1;n||\mathscr{M}(E1)||0\rangle^2 \delta(\omega-\omega_n) = \sum_n B(E1;0\to n)\delta(\omega-\omega_n)\ . \tag{7}$$

The cornerstone of the theoretical approach used here is the polarization tensor introduced in Eq. (2). For the purposes of the present work, the relevant polarization tensor is defined in terms of a time-ordered product of two timelike-isovector densities [see Eq. (3)]. That is,

$$i\Pi^{00}_{33}(x,y) = \langle\Psi_0|T\Big[\hat{\rho}(x)\hat{\rho}(y)\Big]|\Psi_0\rangle = \int_{-\infty}^{\infty} \frac{d\omega}{2\pi} e^{-i\omega(x^0-y^0)} \Pi^{00}_{33}(\mathbf{x},\mathbf{y};\omega)\ . \tag{8}$$

Connecting the nuclear response to the polarization tensor is highly appealing as one can then bring to bear the full power of the many-body formalism into the calculation of an experimental observable [51]. It is worth mentioning that the polarization tensor contains all information about the excitation spectrum of the system. For example, in the uncorrelated case the spectral content of the polarization tensor is both simple and illuminating [51]. The polarization tensor is an analytic function of the excitation energy ω—except for simple poles located at $\omega = \epsilon_p - \epsilon_h$, where $\epsilon_p(\epsilon_h)$ are single-particle (single-hole) energies. Moreover, the residues at these poles correspond to the transition form-factors. Of course, selection rules enforce that only particle-hole excitations with the correct quantum numbers can be excited. To build collectivity into the nuclear response, all these single-particle excitations must be correlated (or mixed) via the residual particle-hole interaction. This is implemented by iterating the uncorrelated polarization tensor to all orders. Such a procedure yields the RPA (Dyson's) equations whose solution embodies the collective response of the ground state [51]. However, the consistency of the MF+RPA approach hinges on the use of a residual particle-hole interaction that is identical to the one used to generate the mean-field potentials. Only then can one ensure the preservation of important symmetries, such as the conservation of the vector current and the decoupling of various spurious modes [47, 52]. A more detailed discussion of the relativistic MF+RPA approach may be found in Ref. [47] (see Ref. [31] for a discussion limited to the dipole response). In the next section results will be presented for the distribution of dipole strength in ^{68}Ni. Particular attention will be placed on the various moments of the distribution and on their relation to the corresponding moments of the photoabsorption cross section. Hence, we close this section with a few essential definitions and relations.

We start by introducing the photoabsorption cross section $\sigma(\omega)$ [23]:

$$\sigma(\omega) = \frac{4\pi^2 e^2}{\hbar c} \sum_n \omega_n \langle 1; n||\hat{D}||0\rangle^2 \delta(\omega - \omega_n) = \frac{16\pi^3}{9} \frac{e^2}{\hbar c} \omega R(\omega) \ . \tag{9}$$

Here $\hat{D}$ is the standard dipole operator and note that the "$E1$" label has been suppressed from $R(\omega; E1)$. Having established the connection between the dipole response and the photoabsorption cross section we now proceed to compute their various moments. These are defined as follows:

$$m_n \equiv \int_0^\infty \omega^n R(\omega) d\omega \ . \tag{10a}$$

$$\sigma_n \equiv \int_0^\infty \omega^n \sigma(\omega) d\omega = \frac{16\pi^3}{9} \frac{e^2}{\hbar c} m_{n+1} \ . \tag{10b}$$

In particular, the photoabsorption cross section satisfies the model independent TRK sum rule (σ_0) which is related to the EWSR (or m_1 moment) as follows:

$$m_1 = \sum_n \omega_n B(E1; 0 \to n) = \frac{9\hbar^2}{8\pi m} \left(\frac{NZ}{A}\right) \approx 14.8 \left(\frac{NZ}{A}\right) \text{fm}^2\text{MeV} \ , \tag{11a}$$

$$\sigma_0 = \frac{16\pi^3}{9} \frac{e^2}{\hbar c} m_1 = 2\pi^2 \frac{e^2}{\hbar c} \frac{(\hbar c)^2}{mc^2} \left(\frac{NZ}{A}\right) \approx 60 \left(\frac{NZ}{A}\right) \text{MeV mb} \ . \tag{11b}$$

We note that the above *classical sum rules* are only valid in the long wavelength approximation (*i.e.,* in the limit in which the photon wavelength is large relative to the nuclear radius) and in the absence of exchange and momentum-dependent forces [23]. Such forces modify the classical sum rules and their impact is traditionally accounted for by multiplying the right-hand side of Eqs. (11) by the factor $(1 + \kappa_{\rm TRK})$, with $\kappa_{\rm TRK} \approx 0.2$ [23]. Also note that the classical sum rules were derived using a non-relativistic formalism so one may also need to correct for relativistic effects. We assume here that such relativistic effects may also be subsumed into $\kappa_{\rm TRK}$ (see Table III). In addition to the fundamental TRK sum rule, a moment of critical importance to the present work because of its sensitivity to the symmetry energy is the *dipole polarizability*. The dipole polarizability is particularly sensitive to low-energy dipole strength given that it is directly proportional to the *inverse* energy weighted sum m_{-1} (or σ_{-2}). That is,

$$\alpha_D = 2e^2 \sum_n \frac{\langle 1; n||\hat{D}||0\rangle^2}{\omega_n} = \frac{\hbar c}{2\pi^2} \sigma_{-2} = \frac{8\pi}{9} e^2 m_{-1} \ . \tag{12}$$

III. RESULTS

We start this section by displaying in Fig. 1 the distribution of dipole strength for the three closed-shell (or at least closed-subshell) nickel isotopes ^{56}Ni, ^{68}Ni, and ^{78}Ni. Predictions are displayed using the accurately calibrated FSUGold (or "FSU" for short) parametrization [53]. In order to resolve individual transitions to bound single-particle states, a small artificial width of 0.5 MeV was included in the calculations. Note, however, that because the *non-spectral* character of our RPA approach [47], particle-escape widths are computed exactly within the model. In panel (a) we display the distribution of dipole strength for the doubly-magic nucleus ^{56}Ni. Predictions for the neutron skin of this $N = Z$ nucleus yield a small negative value of $R_n - R_p = -0.05$ fm because of the Coulomb repulsion among the protons. Consistent with the notion that the Pygmy dipole resonance represents an oscillation of the neutron-rich skin against the symmetric core, no low-energy dipole strength is found. Instead, all the dipole strength is found in the region of the Giant resonance (at excitation energies $\gtrsim$12 MeV) which exhausts 114% of the classical TRK sum rule (*i.e.,* $\kappa_{TRK} = 0.14$). In Fig. 1(b) we observe a significant qualitative change as one moves from ^{56}Ni to the neutron-rich ^{68}Ni isotope. In a mean-field approach such as the one adopted here, the 12 extra neutrons fill in the $1f^{5/2}$, $2p^{3/2}$, and $2p^{1/2}$ orbitals. This leads to the development of a fairly large neutron-skin thickness of $R_n - R_p = 0.21$ fm. Strongly correlated to the development of the neutron skin is the appearance of low-energy dipole strength. Indeed, we now find that 6% of EWSR is contained in the low-energy region. Note that a *model dependent* choice must be made on how to separate the low- and high-energy regions. In the present model—indeed in most MF+RPA models—this separation is natural. Here we define $\omega_t \equiv 11.25$ MeV as the "Pygmy-to-Giant" transition energy [see arrow on Fig. 1(b).] Finally, we display in Fig. 1(c) the distribution of dipole strength for the very exotic ^{78}Ni nucleus. Whereas the additional 10 neutrons filling the $1g^{9/2}$ orbital contribute to a further increase in the thickness of its

neutron skin (from 0.21 to 0.34 fm) the fraction of the EWSR exhausted by the Pygmy resonance actually goes down; from 6% to 4.8%. This *anti-correlation* is reminiscent of the one we reported in Fig. 4 of Ref. [31] for the case of the Tin-isotopes. In the present case, as the *"intruder"* $1g^{9/2}$ orbital is pulled down by the strong spin-orbit force, we observe a mild enhancement of the total EWSR. This enhancement is consistent with the few percent increase in the NZ/A factor as one goes from ^{68}Ni to ^{78}Ni [see Eq. (11)]. However, such an increase is concentrated in the region of the giant resonance because dipole excitations originating in the $1g^{9/2}$ orbital (and ending in the $1h^{11/2}$, $1h^{9/2}$, and $2f^{7/2}$ orbitals) lie high in energy. Thus, we conclude that ^{68}Ni is as good—indeed better—than ^{78}Ni in the search for correlations between the neutron skin and low-energy dipole strength. The same conclusion applies for the case of the Tin isotopes: the *stable* ^{120}Sn isotope may be as useful as ^{132}Sn [31].

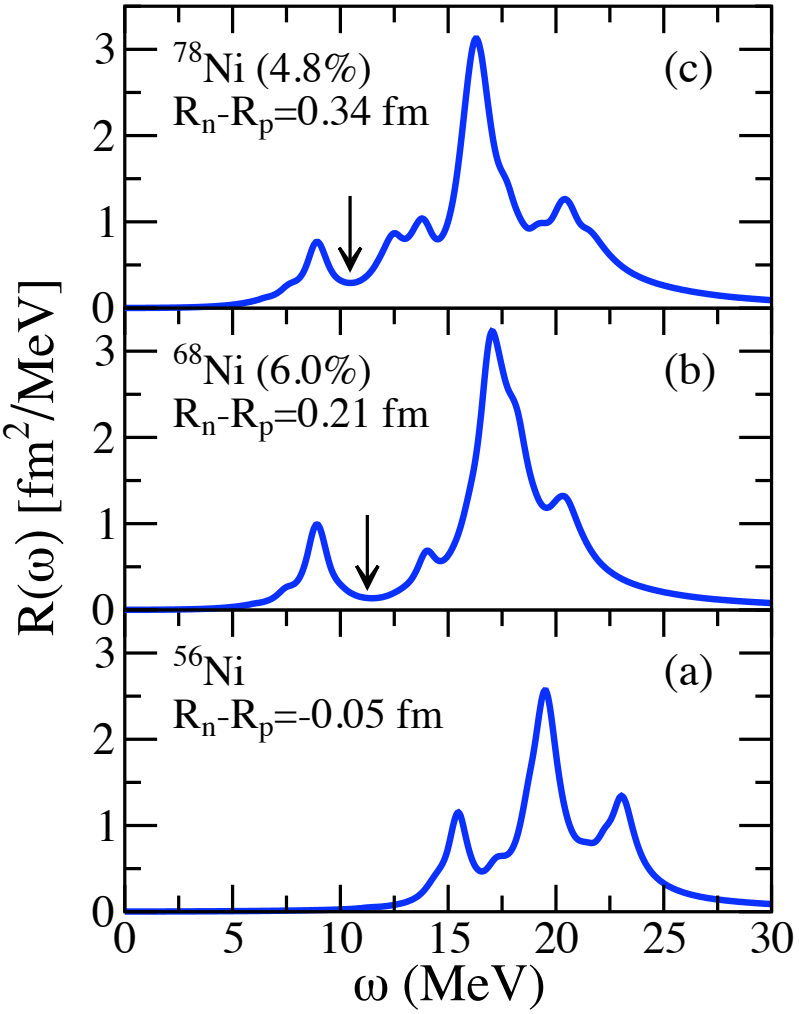

FIG. 1: Distribution of isovector dipole strength for the three closed-(sub)shell nickel isotopes: ^{56}Ni, ^{68}Ni, and ^{78}Ni. Mean field plus RPA predictions are shown using the FSUGold parameter set [53].

To search for correlations between the neutron-skin thickness of ^{208}Pb and the development of Pygmy strength in ^{68}Ni we introduce—in addition to FSUGold [53]—the accurately-calibrated NL3 effective interaction [54, 55]. Parameter sets for these two models are listed in Table I. Although enormously successful in reproducing ground-state energies and charge radii, NL3 predicts equations of state for both symmetric and pure neutron matter that appear too stiff when compared against theoretical and experimental constraints [56–58]. To remedy this deficiency the FSUGold parameter set includes two additional empirical constants, namely, ζ and $\Lambda_{\rm v}$ [see Eq. (1)]. To fully explore the sensitivity of the low energy dipole strength to changes in the neutron-skin thickness of ^{208}Pb we introduce a *"family"* of NL3 and FSUGold models. These families are generated by following a procedure first introduced in Ref. [13]. This procedure is implemented by changing the isovector parameters $\Lambda_{\rm v}$ and g_ρ in such a way that the value of the symmetry energy remains fixed at $\approx$26 MeV at a baryon density of $\approx$0.1 fm^{-3}. This prescription ensures—by construction—that all isoscalar observables remain unchanged. Further, other well constrained observables—such as

masses and charge radii of doubly-magic nuclei—remain consistent with their experimental values. We display in Table II the appropriate isovector parameters $\Lambda_{\rm v}$ and g_ρ for the NL3 and FSUGold families of mean-field interactions. Together with those parameters we display two observables that are particularly sensitive to these changes, namely, the slope of the symmetry energy at saturation density (L) and the neutron skin thickness (R_n-R_p) of both ^{208}Pb and ^{68}Ni (with the latter shown in parenthesis).

Model	$m_{\rm s}$	$m_{\rm v}$	m_ρ	$g_{\rm s}^2$	$g_{\rm v}^2$	g_ρ^2	κ	λ	ζ	$\Lambda_{\rm v}$
NL3	508.194	782.501	763.000	104.3871	165.5854	79.6000	3.8599	−0.015905	0.00	0.000
FSU	491.500	782.500	763.000	112.1996	204.5469	138.4701	1.4203	+0.023762	0.06	0.030

TABLE I: Parameter sets for the two accurately calibrated relativistic mean-field models used in the text: NL3 [54, 55] and FSUGold [53]. The parameter κ and the meson masses $m_{\rm s}$, $m_{\rm v}$, and m_ρ are all given in MeV. The nucleon mass has been fixed at $M=939$ MeV in both models.

To illustrate the role of the various mean-field interactions we display in Fig. 2 the symmetry energy per nucleon predicted by all these models. The density dependence of the symmetry energy is of central importance to this work as it will be used to correlate the neutron-skin thickness of ^{208}Pb to the dipole strength in ^{68}Ni. The symmetry energy represents the susceptibility of the system to changes in the neutron-proton asymmetry. It is defined as follows:

$$S(\rho) = \frac{1}{2}\left(\frac{\partial^2 E(\rho,\alpha)}{\partial \alpha^2}\right)_{\alpha=0} \approx E_{\rm PNM}(\rho) - E_{\rm SNM}(\rho)\ , \tag{13}$$

where $\rho=\rho_n+\rho_p$ is the baryon density of the system and $\alpha=(\rho_n-\rho_p)/\rho$ the neutron-proton asymmetry. As indicated in Eq. (13), the symmetry energy is to a very good approximation equal to the energy of pure neutron matter minus that of symmetric matter. In Fig. 2 the convergence of all models at a density of ≈ 0.1 fm^{-3} (or ≈ 0.7 times the density of nuclear matter at saturation) is clearly discernible. However, the departure from this common value is model dependent. For example, models with a *stiff* symmetry energy—namely, those that change rapidly with density—predict a large slope at saturation density and a correspondingly large value for the neutron-skin thickness of ^{208}Pb. Note that L is proportional to the pressure of pure neutron matter; hence, the larger the value of the neutron pressure the larger the neutron skin. Also note that models with a stiff symmetry energy predict a *lower symmetry energy* at low densities as compared to their softer counterparts. Given that the symmetry energy ($S \propto \partial^2 E/\partial\alpha^2$) acts as the restoring force for isovector modes, we expect that as the symmetry energy stiffens, the distribution of isovector dipole strength will become softer. These arguments suggest how to exploit the behavior of the symmetry energy to correlate the neutron-skin thickness of ^{208}Pb to the dipole strength in ^{68}Ni.

Before doing so, however, we further validate the prescription used to generate the FSU family of mean-field interactions by displaying in Fig. 3 charge and neutron densities for ^{208}Pb (similar results are obtained in the case of NL3). Whereas significant differences are easily discerned in the predictions of the (unknown) neutron density, the model dependence is very small in the case of the charge density. For example, all models predict a mean-square charge radius that is within 0.4% of the experimental value. In the case of the binding energy of ^{208}Pb, the agreement with experiment is even better (by about one order of magnitude). Yet a fairly simple modification to the isovector

Model	$\Lambda_{\rm v}$	g_ρ^2	L (MeV)	R_n-R_p (fm)
NL3	0.00	79.6000	118.189	0.280 (0.261)
	0.01	90.9000	87.738	0.251 (0.241)
	0.02	106.0000	68.217	0.223 (0.222)
	0.03	127.1000	55.311	0.195 (0.203)
	0.04	158.6000	46.607	0.166 (0.183)
FSU	0.00	80.2618	108.764	0.286 (0.265)
	0.01	93.3409	87.276	0.260 (0.248)
	0.02	111.5126	71.833	0.235 (0.223)
	0.03	138.4701	60.515	0.207 (0.211)
	0.04	182.6162	52.091	0.176 (0.189)

TABLE II: The NL3 and FSUGold *"families"* of mean-field interactions. The isovector parameters $\Lambda_{\rm v}$ and g_ρ were adjusted so that all models have the same symmetry energy of ≈ 26 MeV at a density of ≈ 0.1 fm^{-3}. Tuning $\Lambda_{\rm v}$ significantly affects the slope of the symmetry energy at saturation density L and the neutron-skin thickness of ^{208}Pb and ^{68}Ni (the latter shown in parenthesis).

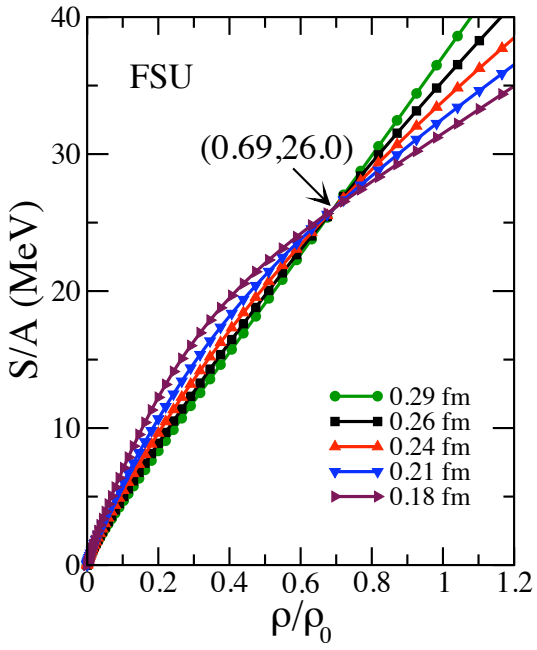

FIG. 2: (Color online) Symmetry energy per nucleon as a function of density (in units of the saturation density). The various effective interactions are labeled according to their predictions for the neutron-skin thickness of ^{208}Pb.

interaction allows one to generate a fairly wide range of values for the neutron-skin thickness of ^{208}Pb: from 0.18 to 0.29 fm.

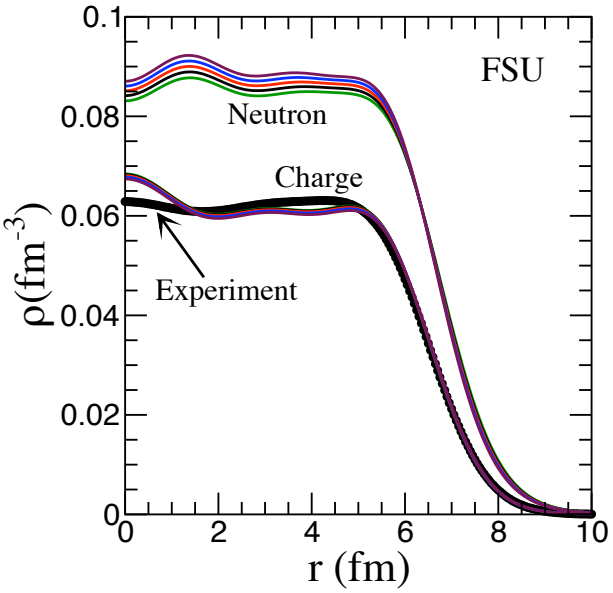

FIG. 3: (Color online) Model predictions for the charge and neutron densities of ^{208}Pb using the FSU family of effective interactions. The experimental charge density is from Ref. [59].

Having validated the choice of mean-field models employed in this work, we now proceed to display in Fig. 4 their predictions for the distribution of dipole strength in ^{68}Ni. Various moments of the distribution as well as the TRK enhancement factor κ_{TRK} [23] have also been collected in Table III. Given that the m_{-1} moment is simply related to the dipole polarizability α_D [see Eq. (12)], it is the latter that is listed in Tables III. Also note that the various curves have been labeled according to their prediction for the neutron-skin thickness of ^{208}Pb. The distribution of strength naturally separates into low-energy (Pygmy) and high-energy (Giant) regions. To compute the contribution

Model	Λ_v	m_1 (fm^{2}MeV)	$\kappa_{\rm TRK}$	m_0 (fm^2)	α_D (fm^3)
NL3	0.00	284.548	0.163	17.428	4.716
	0.01	284.190	0.162	17.151	4.570
	0.02	283.320	0.158	16.832	4.412
	0.03	281.948	0.153	16.454	4.235
	0.04	279.749	0.144	15.984	4.026
FSU	0.00	283.364	0.158	17.270	4.664
	0.01	282.667	0.156	16.976	4.511
	0.02	281.535	0.151	16.627	4.339
	0.03	279.784	0.144	16.199	4.138
	0.04	276.857	0.132	15.635	3.887

TABLE III: Various moments of the distribution of dipole strength $R(\omega)$ for the two families of relativistic mean-field interactions defined in the text. Note that α_D is the dipole polarizability and $\kappa_{\rm TRK}$ denotes the enhancement factor of the TRK sum rule.

from these two regions to the various moments we have selected the Pygmy-to-Giant transition energy to be equal to $\omega_t \equiv 11.25\,$MeV, as indicated in the figure. Note that the dipole strength has been integrated up to a maximum energy of $\omega_{\rm max} \equiv 30\,$MeV. As argued earlier, models with a soft symmetry energy predict large symmetry energies at the low densities of relevance to the excitation of the dipole mode (see Fig. 2). In turn, such a large restoring force generates a significant *hardening and quenching* of the response. That is, models with a soft symmetry predict a distribution of strength that is both hardened (*i.e.*, pushed to higher excitation energies) and quenched relative to their stiffer counterparts. These facts are readily discernible in Fig. 4. We now proceed to explore the consequences of such a hardening and quenching on the various moments of the dipole response.

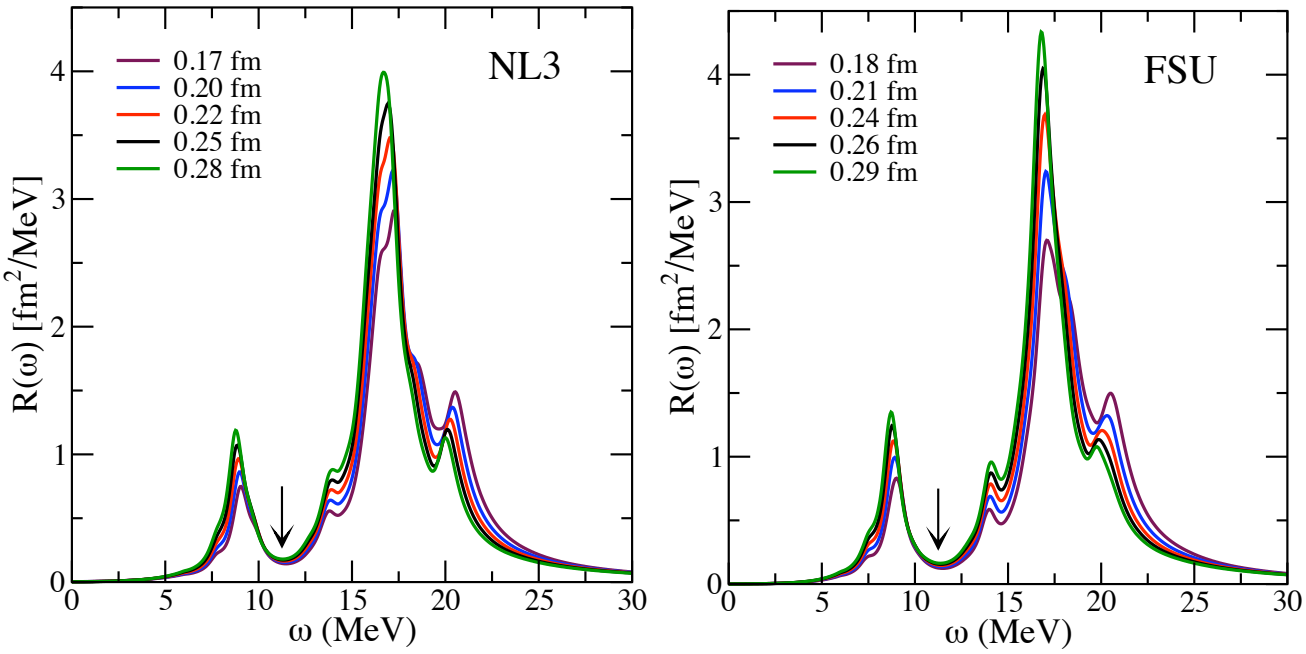

FIG. 4: (Color online) Distribution of dipole strength in ^{68}Ni computed in a MF+RPA approach using the NL3 (left panel) and FSU (right panel) families of effective interactions.

Although the previous discussion suggests a correlation between the neutron-skin thickness of ^{208}Pb and the distribution of dipole strength, the alluded correlation may or may not extend to the various moments of the distribution. This depends critically on whether the quenching and hardening work for or against each other. A prototypical case in which they work against each other is the total m_1 moment, *i.e.*, the energy weighted sum. This expectation is based on the existence of a classical, non-relativistic, and model independent TRK sum rule. That is, we expect that the energy weighting enhances the hardened response as to exactly compensate for its original quenching. To appreciate

Model	Λ_v	E_c (MeV)	m_1 (fm^{2}MeV)	m_0 (fm^2)	α_D (fm^3)
NL3	0.00	8.602	20.680 (7.268)	2.404 (13.794)	1.185 (25.133)
	0.01	8.643	19.231 (6.767)	2.225 (12.973)	1.099 (24.040)
	0.02	8.675	17.713 (6.252)	2.042 (12.130)	1.011 (22.907)
	0.03	8.700	16.074 (5.701)	1.848 (11.229)	0.919 (21.698)
	0.04	8.715	14.248 (5.093)	1.635 (10.227)	0.819 (20.344)
FSU	0.00	8.525	21.592 (7.620)	2.533 (14.666)	1.241 (26.601)
	0.01	8.565	20.185 (7.141)	2.357 (13.883)	1.151 (25.521)
	0.02	8.603	18.628 (6.617)	2.165 (13.023)	1.055 (24.322)
	0.03	8.640	16.871 (6.030)	1.953 (12.054)	0.950 (22.957)
	0.04	8.676	14.732 (5.321)	1.698 (10.861)	0.825 (21.234)

TABLE IV: Contribution from the Pygmy-resonance region ($0 \leq \omega \leq 11.25$ MeV) to the various moments of the distribution of dipole strength. The centroid energy has been defined as $E_c = m_1/m_0$ and the quantities in parenthesis denote the fraction of the total moment contained in the region of the Pygmy resonance.

this fact we display in Fig. 5(a) the energy weighted dipole response $\omega R(\omega)$. Plotted in the inset is the *cumulative* contribution of $\omega R(\omega)$ to the energy weighted sum defined as

$$m_1(\omega) = \int_0^{\omega} \omega' R(\omega') d\omega' \ . \tag{14}$$

The cumulative sum $m_1(\omega)$ displays what appears to be a mild model dependence as it starts to accumulate strength in the region of the Pygmy resonance—with the largest model dependence developing around the main giant-resonance peak. Yet any residual model dependence rapidly disappears as the sum rule is exhausted—as anticipated. However, given that no classical sum rule protects the *fraction* of the energy weighted sum contained in the low-energy region, a model dependence remains. This generates a correlation between the neutron-skin thickness in ^{208}Pb and the fraction of the EWSR exhausted by the Pygmy resonance (see Table IV).

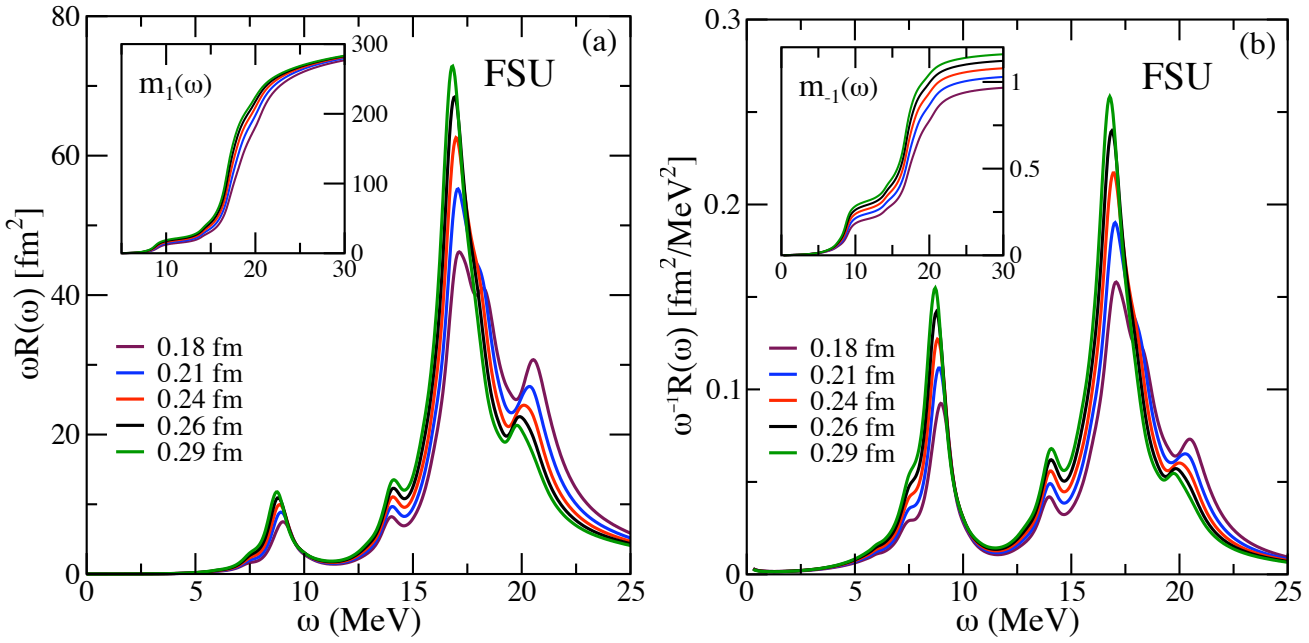

FIG. 5: (Color online) The energy weighted dipole response (a) and the *inverse* energy weighted dipole response (b) in ^{68}Ni computed with the FSU family of effective interactions. The insets display the cumulative sums as defined in Eqs. (14) and (15).

A particularly attractive case in which both the hardening and the quenching work in tandem is the *inverse* energy weighted response $\omega^{-1}R(\omega)$ displayed in Fig. 5(b). First, given that the ω^{-1} factor enhances preferentially the low-energy part of response, the Pygmy resonance now accounts for a significant fraction—of about 20-25%—of the m_{-1}

Model	Λ_v	E_c (MeV)	m_1 (fm^{2}MeV)	m_0 (fm^2)	α_D (fm^3)
NL3	0.00	17.563	263.868 (92.732)	15.024 (86.206)	3.531 (74.867)
	0.01	17.752	264.959 (93.233)	14.926 (87.027)	3.471 (75.960)
	0.02	17.958	265.608 (93.748)	14.790 (87.870)	3.402 (77.093)
	0.03	18.203	265.875 (94.299)	14.606 (88.771)	3.316 (78.302)
	0.04	18.503	265.502 (94.907)	14.349 (89.773)	3.207 (79.656)
FSU	0.00	17.763	261.772 (92.380)	14.737 (85.334)	3.423 (73.399)
	0.01	17.955	262.482 (92.859)	14.619 (86.117)	3.360 (74.479)
	0.02	18.179	262.907 (93.383)	14.462 (86.977)	3.284 (75.678)
	0.03	18.454	262.914 (93.970)	14.247 (87.946)	3.188 (77.043)
	0.04	18.808	262.125 (94.679)	13.937 (89.139)	3.062 (78.766)

TABLE V: Contribution from the Giant-resonance region ($11.25 \leq \omega \leq 30$ MeV) to the various moments of the distribution of dipole strength. The centroid energy has been defined as $E_c = m_1/m_0$ and the quantities in parenthesis denote the fraction of the total moment contained in the region of the Giant resonance.

moment. This should be contrasted against the EWSR where the Pygmy resonance exhausts merely 5-8% of the total sum; see Tables III-V. Second, the inverse energy weighting enhances the softer responses even further. Pictorially, this behavior is best illustrated in the inset of Fig. 5(b) which displays the *cumulative* $m_{-1}(\omega)$ sum:

$$m_{-1}(\omega) = \int_0^\omega \frac{R(\omega')}{\omega'} d\omega' \ . \tag{15}$$

The inset provides a clear indication that both the total m_{-1} moment as well as the fraction contained in the Pygmy resonance are highly sensitive to the neutron-skin thickness of ^{208}Pb. To heighten this sensitivity we display in Fig. 6 the *fractional change* in both the total and Pygmy contributions to the m_1 moment and to the dipole polarizability α_D (we denote these fractional changes with a *"tilde"* in the figure). As alluded earlier, the m_1 moment is fairly insensitive to the density dependence of the symmetry energy (the minor sensitivity is due to differences in the TRK enhancement factors). Instead, the total dipole polarizability is unprotected by a sum rule and changes by about 25% over the range of values span by $R_n - R_p$. This sensitivity and the ensuing strong correlation that emerges between α_D and $R_n - R_p$ is consistent with the results reported in Refs. [38, 60]. However, at least for the class of models employed in this work, the sensitivity of the Pygmy resonance to the neutron-skin thickness of ^{208}Pb is even higher—nearly 50%—for both of the moments.

We closed this section by displaying in Fig. 7 the percentage of the energy weighted sum and of the dipole polarizability exhausted by the Pygmy resonance in ^{68}Ni. In both cases we find these quantities to be strongly correlated to the neutron-skin thickness of ^{208}Pb. The dashed line in Fig. 7(a) represents an upper limit on the fraction of the EWSR of about 6.5% extracted from the analysis of Carbone and collaborators [35]. When combined with the corresponding measurement on ^{132}Sn [34, 36], the same analysis reports values for the neutron skin thickness of ^{208}Pb, ^{68}Ni, and ^{132}Sn of $R_n - R_p = 0.194 \pm 0.024$ fm, 0.200 ± 0.015 fm, and 0.258 ± 0.024 fm, respectively [35]. Note that the accurately-calibrated FSUGold parameter set predicts neutron-skin thickness for these three nuclei of 0.207 fm, 0.211 fm, and 0.271 fm, respectively, which fit comfortably within the above limits. However, although strongly correlated, the FSUGold predictions appear consistently higher than the central values suggested above [35]. This may suggest a symmetry energy even slightly softer than the one predicted by FSUGold. Interestingly enough, astrophysical constraints emerging from the study of neutron-star radii seem to support such a mild softening [61, 62].

IV. CONCLUSIONS

Motivated by two recent publications—one experimental [37] and one theoretical [38]—the distribution of electric dipole strength in the neutron-rich ^{68}Ni isotope was computed using a relativistic RPA approach. Concerning the experimental work, Pygmy dipole strength carrying about 5% of the total energy weighted sum was identified below the main GDR peak [37]. This result is significant as it complements earlier work on the neutron-rich Tin isotopes that suggests a correlation between the fraction of the TRK sum rule exhausted by the Pygmy resonance and the neutron-skin thickness of ^{208}Pb [31, 36]. This validates our earlier claim that models with overly large neutron skins are in conflict with experiment [31]. In regard to the recent theoretical work by Reinhard and Nazarewicz, we find it interesting as it has established a strong correlation between the dipole polarizability and the neutron-skin thickness

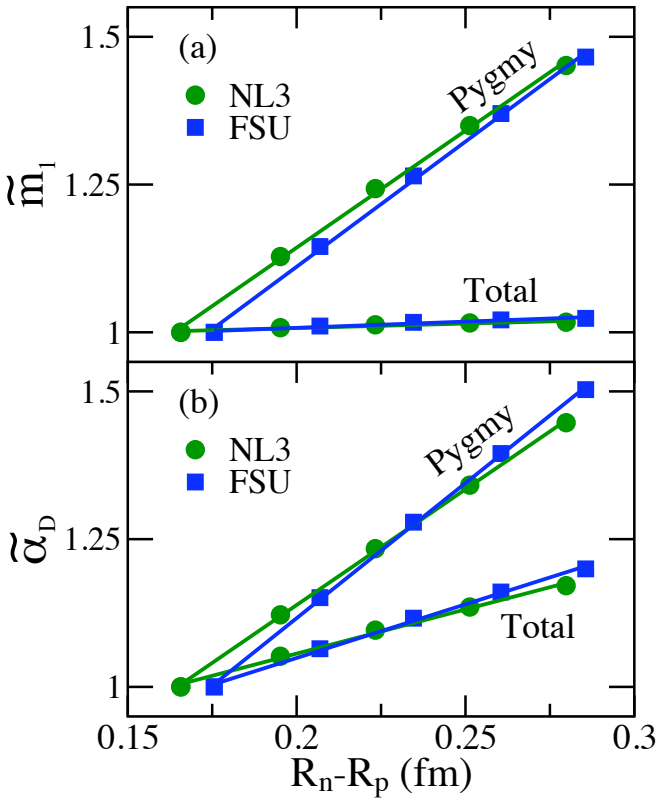

FIG. 6: (Color online) *Fractional change* in the energy weighted sum (a) and dipole polarizability (b) for ^{68}Ni as a function of the neutron-skin thickness of ^{208}Pb.

of ^{208}Pb [38]. As interesting but more intriguing is the claim that the neutron-skin thickness of ^{208}Pb is very weakly correlated with the low-energy electric dipole strength. Such a claim is particularly intriguing given that the dipole polarizability is proportional to the *inverse energy weighted sum* and, as such, the Pygmy resonance should exhaust a large fraction of it. Thus, explaining how can the neutron-skin thickness of ^{208}Pb be strongly correlated to the dipole polarizability but weakly correlated to the Pygmy resonance became a major goal of this project.

To address these issues we relied on a variety of effective interactions that span a wide range of values for the neutron-skin thickness of ^{208}Pb. These effective interactions were derived from accurately calibrated models that were suitably modified by following a procedure first outlined in Ref. [13]. Such a procedure enables one to modify the density dependence of the symmetry energy without compromising the success of the models in describing well constrained nuclear observables.

We have used these models to generate the distribution of dipole strength in ^{68}Ni as well as various moments of the distribution. In particular, values in the 5-8% range were generated for the fraction of the energy weighted sum rule exhausted by the Pygmy dipole resonance. These values seem to fit comfortably within the experimental range reported in Ref. [37]. Hence, by itself, the measurement of low-energy dipole strength in ^{68}Ni does not seem to impose a stringent constraint on the density dependence of the symmetry energy. However, when combined with an earlier experiment on the neutron-rich Tin isotopes [36], the theoretical analysis presented in Ref. [35] argues for a tight constrain on the slope of the symmetry energy (L) that excludes models with both very stiff and very soft symmetry energies. It is significant that such an analysis appears consistent with other approaches—based on nuclear-structure and heavy-ion experiments—that have also been used to constrain L. We note that to these approaches one can add constrains obtained from both low- and high-density physics. Indeed, the equation of state of dilute neutron matter (see Refs. [58, 63] and references therein) as well as neutron-star radii [61, 62] also favor values of L within the range reported in Ref. [35]. In summary, whereas the measurement of the PDR in ^{68}Ni by itself does not impose any stringent constrain on the density dependence of the symmetry energy, it adds consistency to a picture that supports our earlier claim that models with overly large neutron skins are in conflict with experiment [31].

The dipole polarizability played center stage in this contribution because of the expectation that it may act as a surrogate for the neutron skin. Indeed, semi-classical arguments have been used to establish a direct correlation between the neutron-skin thickness and the dipole polarizability [60]. From our perspective, this correlation emerges

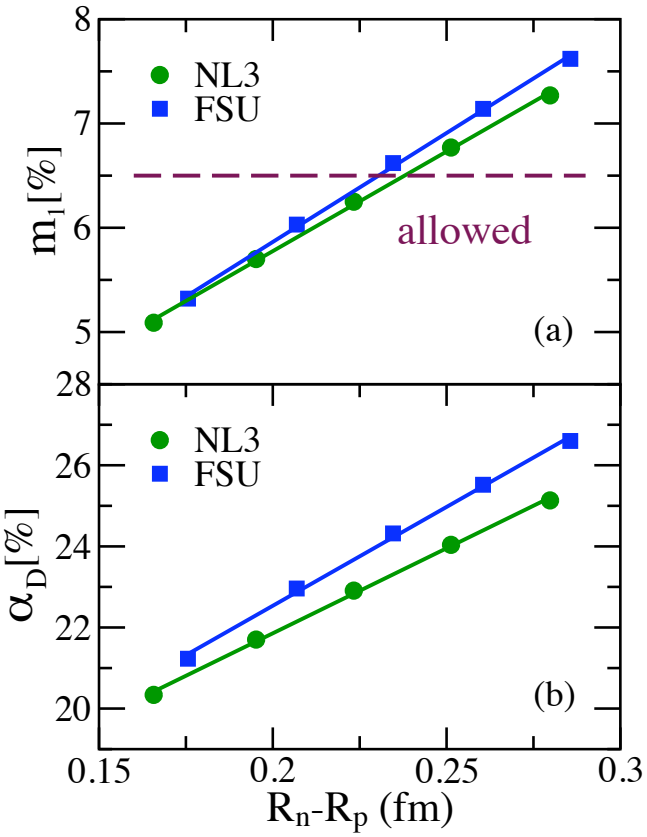

FIG. 7: (Color online) Percentage of the energy weighted sum (a) and dipole polarizability (b) exhausted by the Pygmy dipole resonance in ^{68}Ni as a function of the neutron-skin thickness of ^{208}Pb.

from the realization that the symmetry energy acts as the restoring force of isovector oscillations. As such, models with a soft symmetry energy—and thus a strong restoring force—generate distributions of dipole strength that are both hardened and quenched relative to their stiffer counterparts. And whereas these two effects largely cancel out in the case of the energy weighted sum, they work for each other in the case of the dipole polarizability. This produces a strong linear correlation between the dipole polarizability of ^{68}Ni and the neutron-skin thickness of ^{208}Pb—thereby confirming the assertion of Ref. [38]. But do we also support the claim of a weak correlation between the neutron-skin thickness of ^{208}Pb and low-energy dipole strength? Quite the contrary. To the extent that we can focus on the dipole polarizability, we found a correlation just as strong and an even larger sensitivity. This appears to be a natural consequence of the following two facts: (a) the Pygmy resonance accounts for about 20-25% of the dipole polarizability and (b) the neutron-skin thickness of ^{208}Pb is strongly correlated—with a correlation coefficient of nearly one—to the total dipole polarizability of ^{68}Ni [38]. Note that in our earlier work on the Tin isotopes the centroid energy of the PDR was found to be insensitive to the density dependence of the symmetry energy [31]. There we found, as we do now, centroid energies that are within 2% of each other. This should be contrasted to the nearly 50% sensitivity displayed by the fraction of both the dipole polarizability and EWSR exhausted by the Pygmy resonance. So in an attempt to confirm the assertions of Ref. [38] we obtained mixed results. On the one hand, we confirmed the strong correlation between the dipole polarizability in ^{68}Ni and the neutron-skin thickness of ^{208}Pb. On the other hand, we challenge the view—at least in regard to the dipole polarizability—that the neutron-skin thickness of ^{208}Pb is very weakly correlated to the low-energy dipole strength. Indeed, we suggest that the electromagnetic excitation of both the Pygmy and Giant dipole resonances will continue to provide powerful constraints on the density dependence of the symmetry energy.

Acknowledgments

This work was supported in part by DOE grant DE-FG05-92ER40750.

[1] S. J. Pollock, E. N. Fortson, and L. Wilets, Phys. Rev. **C46**, 2587 (1992).
[2] T. Sil, M. Centelles, X. Vinas, and J. Piekarewicz, Phys. Rev. **C71**, 045502 (2005).
[3] B. A. Brown, Phys. Rev. Lett. **85**, 5296 (2000).
[4] R. J. Furnstahl, Nucl. Phys. **A706**, 85 (2002).
[5] P. Danielewicz, Nucl.Phys. **A727**, 233 (2003).
[6] M. Centelles, X. Roca-Maza, X. Vinas, and M. Warda, Phys.Rev.Lett. **102**, 122502 (2009).
[7] M. Centelles, X. Roca-Maza, X. Vinas, and M. Warda, Phys.Rev. **C82**, 054314 (2010).
[8] M. B. Tsang et al., Phys. Rev. Lett. **92**, 062701 (2004).
[9] L.-W. Chen, C. M. Ko, and B.-A. Li, Phys. Rev. Lett. **94**, 032701 (2005).
[10] A. W. Steiner and B.-A. Li, Phys. Rev. **C72**, 041601 (2005).
[11] D. V. Shetty, S. J. Yennello, and G. A. Souliotis, Phys. Rev. **C76**, 024606 (2007).
[12] M. B. Tsang et al., Phys. Rev. Lett. **102**, 122701 (2009).
[13] C. J. Horowitz and J. Piekarewicz, Phys. Rev. Lett. **86**, 5647 (2001).
[14] C. J. Horowitz and J. Piekarewicz, Phys. Rev. **C64**, 062802 (2001).
[15] C. J. Horowitz and J. Piekarewicz, Phys. Rev. **C66**, 055803 (2002).
[16] J. Carriere, C. J. Horowitz, and J. Piekarewicz, Astrophys. J. **593**, 463 (2003).
[17] A. W. Steiner, M. Prakash, J. M. Lattimer, and P. J. Ellis, Phys. Rept. **411**, 325 (2005).
[18] B.-A. Li and A. W. Steiner, Phys. Lett. **B642**, 436 (2006).
[19] L. Ray and G. W. Hoffmann, Phys. Rev. **C31**, 538 (1985).
[20] L. Ray, G. W. Hoffmann, and W. R. Coker, Phys. Rept. **212**, 223 (1992).
[21] C. J. Horowitz, S. J. Pollock, P. A. Souder, and R. Michaels, Phys. Rev. **C63**, 025501 (2001).
[22] K. Kumar, R. Michaels, P. A. Souder, and G. M. Urciuoli (2005), URL `http://hallaweb.jlab.org/parity/prex`.
[23] M. N. Harakeh and A. van der Woude, *Giant Resonances-Fundamental High-frequency Modes of Nuclear Excitation* (Clarendon, Oxford, 2001).
[24] Y. Suzuki, K. Ikeda, and H. Sato, Prog. Theor. Phys. **83**, 180 (1990).
[25] P. Van Isacker and D. D. Nagarajan, M. A.and Warner, Phys. Rev. **C45**, R13 (1992).
[26] I. Hamamoto, H. Sagawa, and X. Z. Zhang, Phys. Rev. **C53**, 765 (1996).
[27] I. Hamamoto, H. Sagawa, and X. Z. Zhang, Phys. Rev. **C57**, R1064 (1998).
[28] D. Vretenar, N. Paar, P. Ring, and G. A. Lalazissis, Phys. Rev. **C63**, 047301 (2001).
[29] D. Vretenar, N. Paar, P. Ring, and G. A. Lalazissis, Nucl. Phys. **A692**, 496 (2001).
[30] N. Paar, T. Niksic, D. Vretenar, and P. Ring, Phys. Lett. **B606**, 288 (2005).
[31] J. Piekarewicz, Phys. Rev. **C73**, 044325 (2006).
[32] N. Tsoneva, H. Lenske, and C. Stoyanov, Phys. Lett. **B586**, 213 (2004).
[33] N. Tsoneva and H. Lenske, Phys. Rev. **C77**, 024321 (2008).
[34] A. Klimkiewicz et al., Phys. Rev. **C76**, 051603 (2007).
[35] A. Carbone, G. Colo, A. Bracco, L.-G. Cao, P. F. Bortignon, et al., Phys.Rev. **C81**, 041301 (2010).
[36] P. Adrich et al., Phys. Rev. Lett **95**, 132501 (2005).
[37] O. Wieland et al., Phys. Rev. Lett. **102**, 092502 (2009).
[38] P.-G. Reinhard and W. Nazarewicz, Phys.Rev. **C81**, 051303 (2010).
[39] N. Paar, D. Vretenar, E. Khan, and G. Colo, Rept. Prog. Phys. **70**, 691 (2007).
[40] N. Paar, J. Phys. **G37**, 064014 (2010).
[41] H. Mueller and B. D. Serot, Nucl. Phys. **A606**, 508 (1996).
[42] B. D. Serot and J. D. Walecka, Adv. Nucl. Phys. **16**, 1 (1986).
[43] B. D. Serot and J. D. Walecka, Int. J. Mod. Phys. **E6**, 515 (1997).
[44] J. Boguta and A. R. Bodmer, Nucl. Phys. **A292**, 413 (1977).
[45] J. D. Walecka, Annals Phys **83**, 491 (1974).
[46] D. H. Youngblood, H. L. Clark, and Y.-W. Lui, Phys. Rev. Lett. **82**, 691 (1999).
[47] J. Piekarewicz, Phys. Rev. **C64**, 024307 (2001).
[48] J. Piekarewicz, Phys. Rev. **C66**, 034305 (2002).
[49] G. Colò, N. Van Giai, J. Meyer, K. Bennaceur, and P. Bonche, Phys. Rev. **C70**, 024307 (2004).
[50] B. G. Todd and J. Piekarewicz, Phys. Rev. **C67**, 044317 (2003).
[51] A. L. Fetter and J. D. Walecka, *Quantum Theory of Many Particle Systems* (McGraw-Hill, New York, 1971).
[52] J. F. Dawson and R. J. Furnstahl, Phys. Rev. **C42**, 2009 (1990).
[53] B. G. Todd-Rutel and J. Piekarewicz, Phys. Rev. Lett **95**, 122501 (2005).
[54] G. A. Lalazissis, J. Konig, and P. Ring, Phys. Rev. **C55**, 540 (1997).
[55] G. A. Lalazissis, S. Raman, and P. Ring, At. Data Nucl. Data Tables **71**, 1 (1999).

[56] P. Danielewicz, R. Lacey, and W. G. Lynch, Science **298**, 1592 (2002).
[57] J. Piekarewicz, Phys. Rev. **C69**, 041301 (2004).
[58] J. Piekarewicz, J. Phys. **G37**, 064038 (2010).
[59] H. De Vries, C. W. De Jager, and C. De Vries, Atom. Data Nucl. Data Tabl. **36**, 495 (1987).
[60] W. Satula, R. A. Wyss, and M. Rafalski, Phys.Rev. **C74**, 011301 (2006).
[61] A. W. Steiner, J. M. Lattimer, and E. F. Brown, Astrophys.J. **722**, 33 (2010).
[62] F. Fattoyev, C. Horowitz, J. Piekarewicz, and G. Shen (2010), 1008.3030.
[63] A. Gezerlis and J. Carlson, Phys. Rev. **C81**, 025803 (2010).